

# Widar: Decimeter-Level Passive Tracking via Velocity Monitoring with Commodity Wi-Fi

Kun Qian<sup>†</sup>, Chenshu Wu<sup>†</sup>, Zheng Yang<sup>†</sup>, Yunhao Liu<sup>†</sup>, Kyle Jamieson<sup>‡</sup>

<sup>†</sup>School of Software, Tsinghua University, China

<sup>‡</sup>Department of Computer Science, Princeton University, USA

{qiank10,wucs32,hmilyyz,yunhaoliu}@gmail.com,kylej@cs.princeton.edu

## ABSTRACT

Various pioneering approaches have been proposed for Wi-Fi-based sensing, which usually employ learning-based techniques to seek appropriate statistical features, yet do not support precise tracking without prior training. Thus to advance passive sensing, the ability to track fine-grained human mobility information acts as a key enabler. In this paper, we propose *Widar*, a Wi-Fi-based tracking system that simultaneously estimates a **human's moving velocity** (**both speed and direction**) and **location** at a decimeter level. Instead of applying statistical learning techniques, *Widar* builds a theoretical model that geometrically quantifies the relationships between CSI dynamics and the user's location and velocity. On this basis, we propose novel techniques to identify frequency components related to human motion from noisy CSI readings and then derive a user's location in addition to velocity. We implement *Widar* on commercial Wi-Fi devices and validate its performance in real environments. Our results show that *Widar* achieves decimeter-level accuracy, with a median location error of 25 cm given initial positions and 38 cm without them and a median relative velocity error of 13%.

## CCS CONCEPTS

•Human-centered computing →Ubiquitous and mobile computing;

### ACM Reference format:

Kun Qian<sup>†</sup>, Chenshu Wu<sup>†</sup>, Zheng Yang<sup>†</sup>, Yunhao Liu<sup>†</sup>, Kyle Jamieson<sup>‡</sup>. 2017. Widar: Decimeter-Level Passive Tracking via Velocity Monitoring with Commodity Wi-Fi. In *Proceedings of MobiHoc '17, Chennai, India, July 10-14, 2017*, 10 pages.

DOI: <http://dx.doi.org/10.1145/3084041.3084067>

## 1 INTRODUCTION

Location awareness is a key enabler for a wide range of applications such as smart homes, virtual reality, augmented reality, security monitoring, and asset management. Traditional approaches track a user in an active manner via devices such as smartphones or

Permission to make digital or hard copies of all or part of this work for personal or classroom use is granted without fee provided that copies are not made or distributed for profit or commercial advantage and that copies bear this notice and the full citation on the first page. Copyrights for components of this work owned by others than ACM must be honored. Abstracting with credit is permitted. To copy otherwise, or republish, to post on servers or to redistribute to lists, requires prior specific permission and/or a fee. Request permissions from [permissions@acm.org](mailto:permissions@acm.org).

*MobiHoc '17, Chennai, India*

© 2017 ACM. 978-1-4503-4912-3/17/07...\$15.00

DOI: <http://dx.doi.org/10.1145/3084041.3084067>

wearable sensors attached to users [7, 12]. These approaches, however, pose inconvenience since users need to wear or take specific devices and thus are inapplicable in some scenarios such as security surveillance. Other approaches work passively with infrastructure installed in the area of interests, such as cameras and wireless sensor networks (WSNs) [20, 25]. Among them, camera based approaches only provide directional coverage with Line-Of-Sight (LOS) condition and breach user privacy significantly. WSN-based approaches require densely deployed nodes.

Recent innovations in wireless communications shed light on passive human sensing with Wi-Fi signals. Various approaches such as WiVi [3], E-eyes [19], CARM [18] have been proposed for human detection, activity classification, gesture recognition, etc. In principle, these works exploit the phenomenon that human motions distort multipath profiles during signal propagation. These RF based approaches are more attractive than previous solutions since they do not require the user to carry a device, support omnidirectional coverage even in Non-Line-Of-Sight (NLOS) scenarios, and preserve user privacy gracefully.

**Limitations of existing works.** Existing works, however, cannot track fine-grained human mobility information (including speed, direction and location). Specifically, they do not quantitatively model the relationships between signal features and human mobility. Instead, most of them employ learning techniques for gesture and activity recognition by seeking appropriate statistical features of Wi-Fi signals [10, 18, 19]. The key limitations are that they only recognize pre-defined gestures and activities and usually require prior training. Without an elaborate model that outputs locations directly from radio signals, user locations are sometimes identified from recognized specific activities that are highly location-dependent rather than vice versa [19]. Similarly, a user's moving velocity can only be derived from successive locations rather than vice versa. These drawbacks largely confine the application prospects and effects of passive sensing. To advance Wi-Fi-based human sensing, the ability to track fine-grained mobility information from RF signals acts as a fundamental primitive.

**Proposed approach.** In this paper, we proposed *Widar*, a Wi-Fi-based tracking system that simultaneously estimates human's moving velocity and locations at decimeter level. Specifically, we attempt to emulate a Wi-Fi-based velocimeter that measures the instantaneous velocity (both speed and direction), in order to track fine-grained continuous locations. Instead of applying statistical learning techniques, *Widar* achieves these goals by deriving velocities and locations both directly from the Channel State Information (CSI) of Wi-Fi signals [28]. Our key observation is that

movement at different locations with different velocities induces different changes in the lengths of individual signal propagation paths. Therefore, we investigate a CSI-mobility model that captures the geometrical constraints between CSI and a human's location and velocity. On this basis, we propose techniques to extract the rate of change of each signal propagation path length (which we term *path length change rate*, or PLCR), from which we can directly estimate both a user's velocity and location. By doing this, we enable precise tracking of a user's moving velocity and location using COTS Wi-Fi devices.

*Widar* advances the state-of-the-art on Wi-Fi-based sensing from two fronts. First, *Widar* models the relationship between CSI and human mobility from a geometrical perspective, a simpler approach than previous learning based techniques [19]. Such a model helps understand the physical principles of the effects of human mobility on CSI changes. Moreover, our model does not require prior training and can easily generalize to various scenarios. Second, *Widar* directly estimates the velocity of human motion, which is beyond the achievements of existing approaches. Previous works either need to derive velocity from successive location estimates or merely report the mixture of speeds of different body parts [18]. Estimates of moving velocity, as an additional dimension of mobility, stimulate a wide variety of novel applications. For example, velocity analysis provides valuable information for indoor fitness and athletic training.

→ **Challenges and our solutions.** Building such a model and translating it into a practical tracking system involves many challenges. The first challenge is to derive moving velocity from the PLCR. **PLCRs induced by human movements depend on both the location and velocity of the human.** Thus according to the target's specific location, the PLCR is not necessarily equivalent or proportional to the velocity. A huge gap exists between CSI and velocity, although existing models have associated CSI with motion-induced propagation path changes [18]. In our work, we attempt to bridge this gap and further extend to simultaneous estimation of moving velocities and locations. To achieve this, a quantitative model is required to precisely depict the physical constraints of CSI changes and the user's location and velocity.

The second challenge is to **determine signs of PLCRs that indicate moving direction. With only absolute PLCR**, it is difficult to tell whether a reflector is moving towards or away from the link. Considering the simplest case where a user moves along the extended line of a transmitter and a receiver, a movement of 0.5m either towards or backwards the link both causes an identical change of 1m in reflecting path length. To fully eliminate such direction ambiguity, we integrate recent art [23], which enables estimation of signs of PLCR in restricted moving directions provided sufficiently long observations, to opportunistically identify signs of PLCRs for particular links and search through the space of possible signs for the other links using a **novel error function based on the continuity of sequential locations**.

The third challenge is to **identify moving velocity from the superpositioned reflections from different human body parts**. For the purpose of tracking a user's location, we mainly care about the moving velocity. However, motion of different body parts (e.g., arms and legs) all potentially contribute to CSI changes, adding non-negligible changes to PLCRs. Hence, *Widar* needs to distinguish

the mixed components and identify the relevant parts for velocity estimation. To achieve this, we propose a novel PLCR extraction algorithm based on dynamic programming to identify the targeted frequency components.

Overcoming all these challenges, *Widar* enables precise tracking of both human locations and velocities with CSIs. We implement *Widar* on COTS Wi-Fi devices and conduct extensive experiments in real world. The results demonstrate that *Widar* yields decimeter-level tracking with a respective median location error of 25 cm and 38 cm with and without initial positions and a mean relative velocity error of 13%.

In a nutshell, our core contributions are as follows: First, we build a geometrical model that captures the relationships of CSI dynamics and human mobility, which underpins the feasibility of human sensing without a training phase. Second, we design a system that simultaneously and directly tracks human moving velocity (both speed and direction) and location, which provides us richer mobility information for various applications. We envision this capability as a key enabler for future motion recognition applications. Third, we implement *Widar* and validate its performance on COTS hardware. Experimental results show that *Widar* achieves a decimeter-level accuracy with only one commercial Wi-Fi sender and two receivers.

## 2 PRELIMINARY

This section provides a primer on CSI and state-of-the-art model relating CSI dynamics with human movement. The limitations and challenges of adapting the existing model to passive human tracking are discussed.

### 2.1 Channel State Information

Taking multipath propagation into consideration, the wireless channel has the following structure at frequency  $f$  and time  $t$ :

$$H(f, t) = \sum_{k=1}^K \alpha_k(t) e^{-j2\pi f \tau_k(t)}, \quad (1)$$

where  $K$  is the total number of multipath components.  $\alpha_k(t)$  and  $\tau_k(t)$  are the complex attenuation factor and propagation delay for the  $k$ -th path respectively. CSI, provided as a software API by off-the-shelf Wi-Fi NICs, is a discretely sampled version of channel response in time-frequency space [4]. In the frequency domain, CSI is sampled on certain OFDM subcarriers, while in time domain, CSI is measured for each received 802.11 frame.

### 2.2 From CSI to PLCR

Relative movements between transceivers and reflectors lead to **Doppler effect**, which shifts the frequency of the signal for observers, as discussed in prior work [10, 15]. The root cause of Doppler frequency shifts is the change in the length of the signal propagation path [18]. As shown in Figure 1a, the frequency shift of the signals reflected off the moving human is given by:

$$f_D(t) = -\frac{1}{\lambda} \frac{d}{dt} d(t) = -f \frac{d}{dt} \tau(t), \quad (2)$$

where  $\lambda, f, \tau(t)$  are the wave-length, carrier frequency and time of flight of the signal, and  $d(t)$  is the length of the path NLOS, and the PLCR  $r$  is mathematically defined as  $r \triangleq \frac{d}{dt} d(t)$ .



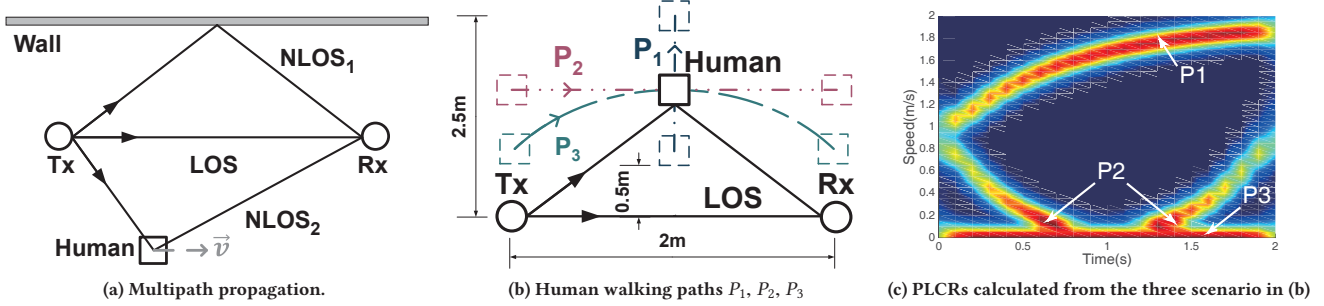


Figure 1: Typical movement and its effect on the path length change rate (PLCR).

Thus, CSI can be represented as superimposition of path responses modulated by Doppler frequency shift arising from moving reflectors on each path:

$$H(f, t) = (H_s(f) + \sum_{k \in P_d} \alpha_k(t) e^{j2\pi \int_{-\infty}^t f_{D_k}(u) du}) e^{-jk(f, t)}, \quad (3)$$

where  $H_s(f)$  is the sum of responses for static paths ( $f_D = 0$ ),  $P_d$  is the set of dynamic paths ( $f_D \neq 0$ ). However, CSI is polluted by unknown phase shifts  $\kappa(f, t)$ , which is caused by residue frequency and time offsets of imperfect hardwares. To eliminate the unknown shift, CARM [18] calculates the CSI power (i.e. conjugate multiplication of CSI) and extract PLCR through frequency domain.

### 2.3 Challenges for Tracking

The model described above is helpful for activity recognition when approximating human velocity as a fixed function of PLCR, which is, however, insufficient for tracking. To track with CSI, three challenges exist.

**From PLCR to target velocity.** As PLCR only reflects the Doppler frequency shifts, it is not real velocity of the moving target. Instead, both target velocity and location jointly determine the PLCR of the target reflecting path. For example, as depicted in Figure 1b, target  $P_1$  is on the perpendicular bisector of the link;  $P_2$  is parallel with the link;  $P_3$  is on an ellipse whose foci are the transmitter and receiver. Suppose an identical constant velocity and the same length of each trace, we plot their respective PLCRs in Figure 1c, which turn out to be significantly different from each other. In conclusion, while PLCR provides some clues of human motion, it can not directly measure movement. An advanced model that outputs human mobility information from PLCRs is needed for tracking.

**Loss of the sign.** While CSI power excludes unknown phase offsets, it also loses the sign of frequency shifts due to conjugate multiplication. Recall Equation 2, the sign of frequency shift is identical to that of PLCR, which indicates whether the reflector moves towards or away from the link. Without the sign information, it is unable to obtain moving directions and further track locations with velocities.

**Interference terms.** As shown in Equation 3, CSI contains irrelevant multipath components, the CSI power, as conjugate multiplication of itself, may contain irrelevant cross-terms, unwanted frequency shift terms and time-variant power terms that severely

interfere with the targeted frequency shift components for tracking. Specifically, when a person walks, not only the torso but also other moving body parts reflect significant signal power, resulting in multiple reflection components. To obtain movement velocity, we need to eliminate disturbances of irrelevant body parts as well as other sources of interference and retain only the relevant components among the superimposed observations.

## 3 MODELING OF CSI-MOBILITY

In this section, we attempt to build a model to directly relate CSI dynamics to human moving velocity together with location. We achieve this by considering the geometrical constraints between reflection paths and human movement. We start with the ideal case where the sign of PLCR is available, and then extend to the practical case without such knowledge.

### 3.1 The Ideal Model

When a target moves, only certain velocity components affect reflecting path lengths, and thus influence the corresponding PLCR. As shown in Figure 2a, taking the transmitter and receiver as ellipse foci, the length of reflecting path decides which ellipse the target is on. The target velocity  $\vec{v}$  can be decomposed into a radial velocity  $\vec{v}_r$  and an orthogonal tangential velocity  $\vec{v}_t$ . While the tangential velocity  $\vec{v}_t$  does not affect the reflection path length, the radial velocity  $\vec{v}_r$  moves the target away from the ellipse and induces change in the reflection path length. As a result, only the radial velocity  $\vec{v}_r$  can be deduced from PLCR, and target velocity cannot be uniquely identified. For example, in Figure 2a,  $\vec{v}'$  and  $\vec{v}$  (which share the same radial velocity component) cannot be distinguished with the only knowledge of  $\vec{v}_r$ .

Fortunately, we are able to solve the ambiguity and derive the true velocity with more links, which add further geometric constraints. For example, by adding one more link (Figure 2b), the target velocity  $\vec{v}$  can be deduced from  $\vec{r}_1$  and  $\vec{r}_2$ , as long as the two radial velocities are not in the same direction. Thus, ideally, at least two links are required to calculate the target velocity. Furthermore, by adding more links (Figure 2c), the optimal solution,  $\vec{v}_{opt}$ , can be even calculated in case of measurement errors in PLCRs.

Given the position of the transmitter and the receiver of the  $i$ -th link as  $\vec{l}_t^{(i)} = (x_t^{(i)}, y_t^{(i)})^T$ ,  $\vec{l}_r^{(i)} = (x_r^{(i)}, y_r^{(i)})^T$ , the current target position as  $\vec{l}_h = (x_h, y_h)^T$ , the target velocity as  $\vec{v} = (v_x, v_y)^T$ ,

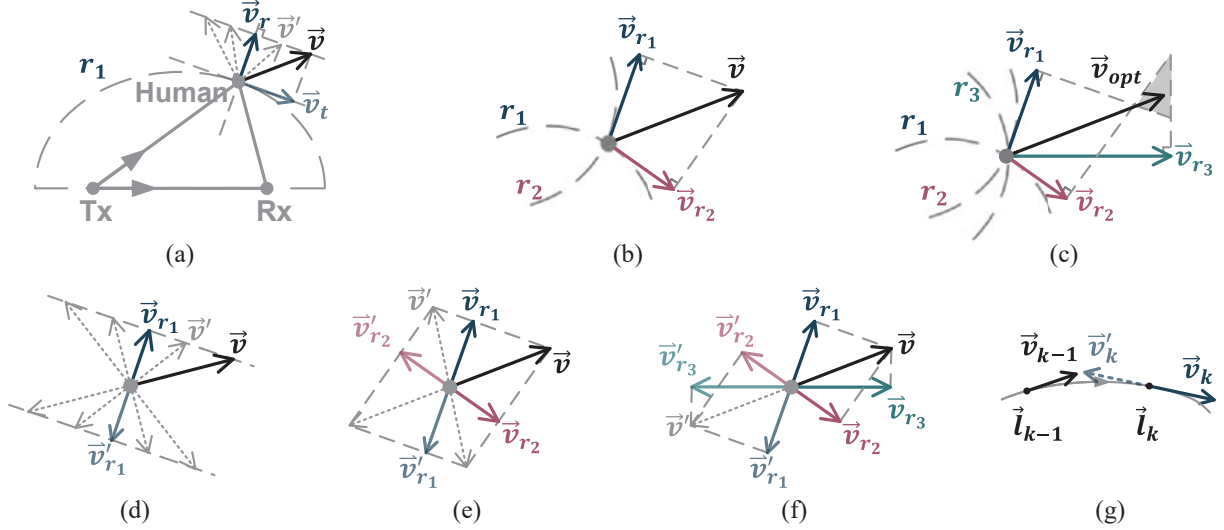


**Figure 2: Relation between target velocity and PLCR: the model with information of the sign of PLCR: (a)one link, (b)two links, (c)three links; the model without the sign information: (d)one link, (e)two links, (f)three links; and (g)consecutiveness of target movements.**

and PLCR as  $r^{(i)}$ , the PLCR can be algebraically represented by the target velocity:

$$a_x^{(i)}v_x + a_y^{(i)}v_y = r^{(i)}, \quad (4)$$

where

$$\begin{aligned} a_x^{(i)} &= \frac{x_h - x_t^{(i)}}{\|\vec{l}_h - \vec{l}_t^{(i)}\|} + \frac{x_h - x_r^{(i)}}{\|\vec{l}_h - \vec{l}_r^{(i)}\|}, \\ a_y^{(i)} &= \frac{y_h - y_t^{(i)}}{\|\vec{l}_h - \vec{l}_t^{(i)}\|} + \frac{y_h - y_r^{(i)}}{\|\vec{l}_h - \vec{l}_r^{(i)}\|}. \end{aligned} \quad (5)$$

Aggregating relations of all  $L$  links, we have:

$$\mathbf{A}\vec{v} = \vec{r}, \quad (6)$$

where

$$\begin{aligned} \mathbf{A} &= \begin{pmatrix} a_x^{(1)} & a_x^{(2)} & \dots & a_x^{(L)} \\ a_y^{(1)} & a_y^{(2)} & \dots & a_y^{(L)} \end{pmatrix}^T, \\ \vec{r} &= \begin{pmatrix} r^{(1)} & r^{(2)} & \dots & r^{(L)} \end{pmatrix}^T. \end{aligned}$$

The optimal solution for  $\vec{v}$  can then be expressed in terms of  $\mathbf{A}$  and  $\vec{r}$ :

$$\vec{v}_{\text{opt}} = (\mathbf{A}^T \mathbf{A})^{-1} \mathbf{A}^T \vec{r}. \quad (7)$$

### 3.2 The Real Model

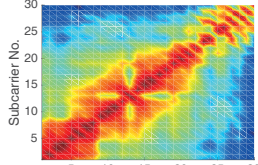
The above elegant result, however, does not hold in practice when the signs of PLCRs are unknown. As shown in Figure 2d, with only the absolute PLCR value from one link, the target may move in any direction other than the pair of tangential directions. With one link added (Figure 2e), the number of velocity candidates reduces to four, since there are in total four possible combinations of two unsigned radial velocities of the two links. Adding another link (Figure 2f) further excludes a pair of candidates with larger fitting errors. However, further adding any number of extra links does

not solve the ambiguity of the remaining pairs of candidates, in that all constraints (i.e. absolute PLCRs) added by additional links are fulfilled by the two candidates due to central symmetry, as in Figure 2f.

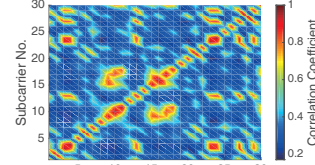
Fortunately, such symmetrical ambiguity can be resolved as long as the sign of PLCR of any link is known. Recent art, WiDir [23], proposes to identify the sign of PLCR through time lags of signal variations of CSI subcarriers. **The key insight is that different subcarriers experience non-zero time lags in motion-induced signal variations due to their slightly different wavelengths**. Specifically, as the target moves towards a link, subcarriers with larger wavelengths experience constructive variations earlier than those with smaller wavelengths, while later as the target moves away from the link. Thus, the signs of PLCR could be inferred by inspecting signs of the time lags.

However, **WiDir has two major limitations**: 1) The calculated time lag is unstable due to severe noises and thus long duration data is required to statistically identify the correct sign of PLCR. 2) Even with sufficient data, **WiDir fails to identify the sign of PLCR** when the target moves in approximately parallel with the link due to evenly distributed time lags in such case. Thus, *Widar* integrate WiDir to opportunistically obtain hints of signs of PLCR.

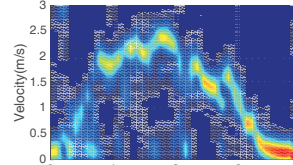
To fully resolve the ambiguity of solutions, we further introduce constraints based on the continuity of target movement in the real world. Specifically, for human movement, the directions of consecutive velocities within a certain small time interval (e.g. 100 ms), are likely to be similar, due to natural limitations on people's moving accelerations and the high sampling rates supported by commercial devices. Figure 2g illustratively demonstrates the effect of the constraint. Suppose the last measurement of target velocity is  $\vec{v}_{k-1}$ . At time  $k$ , for the two symmetric velocity candidates,  $\vec{v}_k$  and  $\vec{v}'_k$  with the smallest fitting error,  $\vec{v}_k$  holds a significantly higher probability to be the current velocity since it is almost in



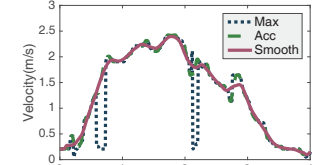
(a) Walking



(b) Standing



(a) Spectrogram



(b) PLCRs

**Figure 3: Cross-correlation of subcarriers when a person walks and stands still**

the same direction as preceded  $\vec{v}_{k-1}$ . Based on this insight, we design an effective model to derive continuous velocities of human movements from PLCRs extracted from CSI measurements.

Denote the sign of PLCR of the  $i$ -th link at time  $k$  by  $s_k^{(i)}$ , where  $s_k^{(i)} \in \{-1, 1\}$  is either decided by WiDir, or an unknown binary variable. Then Equation 6 has following transformation:

$$\mathbf{A}_k \vec{v}_k = \mathbf{R}_k \vec{s}_k, \quad (8)$$

where

$$\begin{aligned} \mathbf{R}_k &= \text{diag} \left( |r_k^{(1)}|, |r_k^{(2)}|, \dots, |r_k^{(L)}| \right), \\ \vec{s}_k &= \left( s_k^{(1)}, s_k^{(2)}, \dots, s_k^{(L)} \right)^T. \end{aligned}$$

And the optimal solution for  $\vec{v}_k$  becomes:

$$\vec{v}_{k,\text{opt}} = (\mathbf{A}_k^T \mathbf{A}_k)^{-1} \mathbf{A}_k^T \mathbf{R}_k \vec{s}_k. \quad (9)$$

The optimal solution for  $\vec{s}_k$  can be obtained by minimizing following error function:

$$\begin{aligned} \vec{s}_{k,\text{opt}} &= \underset{\vec{s}_k \in \{-1, 1\}^L}{\operatorname{argmin}} (\text{err}_{l,k} + \beta \cdot \text{err}_{v,k}), \\ \text{err}_{l,k} &= \|\mathbf{A}_k \vec{v}_{k,\text{opt}} - \mathbf{R}_k \vec{s}_k\|, \\ \text{err}_{v,k} &= \|\mathbf{A}_k \vec{v}_{k,\text{opt}} - \mathbf{A}_{k-1} \vec{v}_{k-1,\text{opt}}\|, \end{aligned} \quad (10)$$

where  $\text{err}_{l,k}$  is the mean square error that quantifies inconsistency between PLCR and solved velocity.  $\text{err}_{v,k}$  is the velocity deviation error that quantifies the deviation of current velocity against to last velocity estimation.  $\beta$  is the weight factor to prevent excessive impact of the error term  $\text{err}_v$ . The rationality lies in that the optimization procedure determines two best fitted candidates mostly based on the mean square error while applies the second velocity deviation error term to exclude one of them.

Unlike traditional models, our CSI-Mobility model geometrically relates PLCR to moving velocities and locations, which shows the feasibility of simultaneous tracking of velocity and location even using only three links.

## 4 PLCR EXTRACTION

This section presents processes for extracting PLCRs and their signs. Illustrations of the processes are calculated from field-test data, as in Section 6.1. To extract PLCRs from noisy and interfered CSIs, Widar first preprocesses the CSI sequence to obtain noisy spectrogram of signals with a target frequency shift. Then, a novel extraction algorithm based on the constraint of target acceleration

**Figure 4: Extraction of PLCRs with a person walking in straight line**

is applied to the spectrogram to finally retrieve target PLCR. To efficiently extract signs of PLCRs, Widar implements cross correlation and time lag identification in frequency domain.

### 4.1 CSI Preprocessing

**Passband filtering.** Comparing to frequency of reflecting signals caused by human movement, the frequency of impulses and burst noises is generally higher, and the frequency of interference caused by static and quasi-static reflectors and the LOS signal is generally lower. Thus, it is natural to suppress these uninteresting signal components with filters. Specifically, we adopt a Butterworth filter (with cutting off frequency set to 2 Hz and 80 Hz respectively) for its flat amplitude response in passband that does not distort target signal components, and apply filters to all subcarriers of CSI power series  $|H(f, t)|^2$  to eliminate independent noises and interference in each subcarrier.

**Subcarrier selection.** Figure 3 shows correlations of CSI power segments of different subcarriers in typical scenarios where human moves and stands still in the monitor area. When the human moves, all OFDM subcarriers experience similar power variations caused by the reflecting signal, and have a statistically higher degree of correlation than in static scenario. However, some subcarriers may experience weaker power variations due to reflector motions, and are more vulnerable to correlated noises. It inspires us to design a correlation-driven selection strategy to choose appropriate subcarriers to increase the proportion of reflecting power while suppress irrelevant noise. Specifically, we split the CSI power series into overlapped 0.5 s segments. For segments with moving targets, we select first 20 subcarriers which have larger increases in correlation coefficients relative to latest static segments. Then, we perform Principal Component Analysis (PCA) on the selected group of subcarriers and select the first PCA component for time-frequency analysis. Thanks to subcarrier selection and PCA based extraction, the first PCA component contains major and consistent power variations caused by all target motions.

**Time-frequency Analysis.** To efficiently estimate PLCR at stable resolution across both frequency and time, we apply STFT to the first PCA component. For each segment of the PCA series, a 0.125 s Gaussian window is applied to smooth the spectrogram and a 0.5 s zero padding is added to achieve finer frequency resolution of 1 Hz. Finally, the non-overlapping spectrograms of all segments are spliced together to generate the whole PLCR spectrogram (Figure 4a).

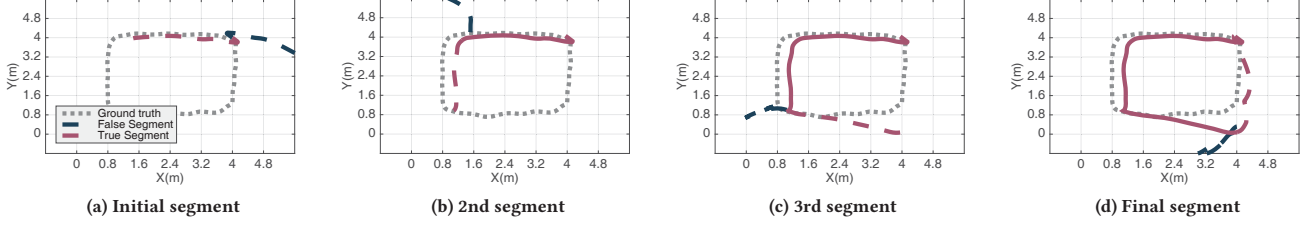


Figure 5: Illustration of trace segmentation and refinement for a long trace

## 4.2 PLCR Extraction Algorithm

The human torso reflects more signals than other body parts, leading to dominant components in spectrogram. Thus, we could select frequency bins with maximum power as the PLCRs caused by human movements. In practice, however, this yields significant errors (Figure 4b), since the spectrogram may contain abnormal fluctuations due to remnant noises and interferences in the passband.

To remove noise and interference in such situation, we propose an extraction algorithm based on the acceleration constraints of path length change. Since the acceleration  $a$  and Doppler frequency shift  $f_D$  has following relation:

$$a(t) = \frac{d^2}{dt^2} d(t) = \lambda \frac{d}{dt} f_D(t), \quad (11)$$

with the knowledge of the maximum acceleration of walking human [29], we can properly decimate the spectrogram in time domain to limit the frequency change in adjacent time samples to a single frequency bin. For convenience of programming, we adopt a relaxed value of  $3.2 \text{ m/s}^2$  as the maximum acceleration, and accordingly, we set the upper bound of acceleration of path length change to  $a_m = 6.4 \text{ m/s}^2$ . As the frequency resolution of the spectrogram is  $\Delta f = 1 \text{ Hz}$ , we decimate the spectrogram to sampling rate of  $f_s = 128 \text{ Hz}$ . Instead of selecting the strongest bin at each time point, we maximize the overall power of the whole trajectory.

Denote the spectrogram as  $W_{T \times F}$ , where  $F$  is number of frequency bins and  $T$  is number of time bins. The optimal PLCR, as the function of indices of frequency bins, can be solved via the following dynamic programming problem:

$$\begin{aligned} \text{PLCR}_{\text{opt}} &= \text{PLCR}(\underset{f_1, \dots, f_T}{\operatorname{argmax}} \sum_{i=1}^T W_{i, f_i}), \\ \text{s.t. } |f_i - f_{i-1}| &\leq 1; i = 2, \dots, T. \end{aligned} \quad (12)$$

Upon obtaining the PLCR series, we apply a moving average window to the series to further smooth the data (Figure 4b).

## 4.3 PLCR Sign Identification

After extraction of PLCR, *Widar* tries to identify the sign of PLCR. Instead of calculating cross covariance that may suffer from variations of absolute signal power as in [23], *Widar* calculates cross correlation between subcarriers for time lags. Specifically, for each PLCR sample, *Widar* calculates time lags between subcarrier segments around the sample. Denote  $s(t, T)$  as the segment whose center time is  $t$  and interval length is  $T$ . For subcarriers  $s_1, s_2$ , the

cross correlation function  $R(\tau)$  is calculated as:

$$R(\tau) = \frac{\mathcal{F}^{-1}\{\mathcal{F}\{s_1(t, 2T)\} \cdot \mathcal{F}^*\{s_2(t, 2T)w(t)\}\}(t + \tau)}{\|s_1(t + \tau, T)\| \cdot \|s_2(t, T)\|}, \quad (13)$$

$$-\frac{T}{2} \leq \tau \leq \frac{T}{2}$$

where  $\mathcal{F}$  is Fourier transform, and  $w(t)$  is a window function that is 1 within interval  $[t - \frac{T}{2}, t + \frac{T}{2}]$  and 0 elsewhere. The key advantage of cross correlation in frequency domain lies in its computational efficiency compared with that in time domain. Specifically, the calculation of numerator only involves Fourier transform and dot product, while calculation of denominator can be carried out iteratively in linear time. Thus the calculation of cross correlation only requires only  $O(T \log T)$  time cost. *Widar* adopts  $T = 0.125 \text{ s}$  CSI segment and calculates time lags between subcarriers spacing every 5 indices, as recommended in [23].

However, since the calculated time lag is unstable, *Widar* accumulates time lags as PLCR is above a threshold (e.g.  $0.5 \text{ m/s}$ ), and calculates the distribution of signs once PLCR decreases below the threshold or until enough time lags has been accumulated (e.g.  $3 \text{ s}$ ). The signs of continuous PLCRs are opportunistically identified if the percentage of specific sign exceeds a threshold (e.g.  $70\%$ ). The rationality behind such operation is that when the sign of PLCR changes, the PLCR must cross zero line and a significant decrease in PLCR can be observed. In contrast, continuous large PLCRs are likely to have the same signs.

## 5 TRACKING VELOCITY & LOCATION

To fully track human velocity as well as location, *Widar* has to detect human movement, pinpoint the human to provide initial target location and successively update his velocity and location. Lacking external information for references, *Widar* further adopts a pseudo self-calibration scheme and an antenna selection criterion to refine tracking results.

### 5.1 Movement Detection

Velocity estimation should be performed only when a person is walking nearby. To detect the start and end of human walking, *Widar* makes two key observations. First, as in Figure 3, the correlation between different subcarriers increases in the presence of human walking. Second, when a human is walking, the spectrogram power concentrates at certain frequencies corresponding to the signal reflected by the human body; otherwise, the power

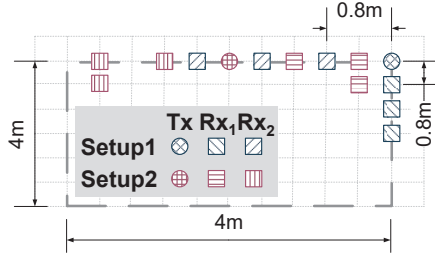
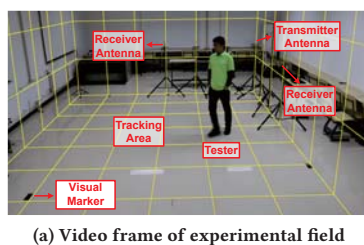
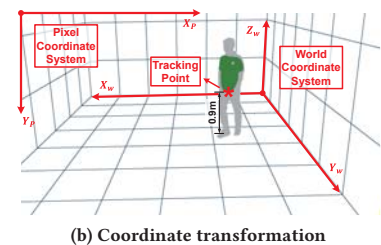


Figure 6: Deployment schemes of Widar.



(a) Video frame of experimental field



(b) Coordinate transformation

Figure 7: Obtaining ground truth via visual videos

distribution of the spectrogram is dispersed. In practice, *Widar* continuously monitors the environment, and calculates the mean cross-correlation value  $C$  and mean normalized variance  $\sigma^2$  of power distribution of frequency spectrum. The movement detection indicator (MDI) is then defined as  $Ce^{-(\sigma^2 - \sigma_m^2)}$ , where  $\sigma_m^2$  is the minimum variance observed in last two seconds before user starts moving. Only when MDI exceeds the predefined location-independent threshold does *Widar* start to track human movement.

## 5.2 Initial Location Estimation

*Widar* tracks human movements with velocity, rather than location estimations. Consequently, an initial location is needed. There exists approaches for passive localization [8, 16], which however are not directly feasible for scenarios of *Widar*. LiFS [16] requires dense deployment of devices to ensure targets always sufficiently close to the LoS of some links. Dynamic-Music [8] requires pre-calibration of NICs and strictly shaped antenna array. To complement the tracking process while avoiding learning and training, *Widar* provides an alternative approach through a quick-and-dirty location search. Specifically, *Widar* first searches through the whole tracking area at a coarse resolution, identifying a location that yields the least fitting error of the trace, as the initial location. Then, *Widar* searches through the narrowed area around the initial location at a fine-grained resolution to refine the initial location accuracy. This search step can be iterated until the fitting error achieves the minimum.

## 5.3 Successive Tracking

As the initial direction at the start point is unknown, we set  $\vec{v}_0$  as a small disturbance that takes values in a pair of symmetric vectors (e.g.  $(0.01, 0.01)^T$  and  $(-0.01, -0.01)^T$ ).

Upon obtaining current velocity  $\vec{v}_{k,\text{opt}}$  using Equation 10, the target location can be updated as:

$$\vec{l}_{k+1} = \vec{l}_k + \vec{v}_{k,\text{opt}} \cdot \Delta t, \quad (14)$$

where  $\Delta t$  is the interval between two consecutive measurements. And the target velocity thereafter can be successively estimated in the same way.

## 5.4 Trace Refinement

**Pseudo-calibration.** Opportunistic location hints are necessary for calibration in a tracking system to avoid accumulative errors. Since we do not have extra information to serve as precise initial

locations and for calibration, we employ a pseudo-calibration approach based on trace segmentation to refine the tracking results and remove erroneous trajectories.

As shown in Figure 5, we observe that *Widar* may misjudge the velocity direction in some cases, especially when the user takes a sharp turn or walks very slowly. To avoid error accumulation due to such mistakes, we first perform trace segmentation at these vulnerable moments and re-initialize the tracking process for each new segment to guarantee the correct direction.

**Antenna selection.** During real tracking, we observe that some links yield wrong PLCRs due to weak reflecting signal-to-noise ratio and small PLCR itself, which may lead to totally wrong trace. To pick out these “bad” antennas, *Widar* adopts two-round tracking for each trace segment. In the first round, least square method (Equation 9) is used to calculate optimal velocity. In the second round, a weight is applied to the least square method in order to suppress “bad” antennas:

$$\vec{v}_{k,\text{opt}} = (A_k^T W A_k)^{-1} A_k^T W \vec{s}_k. \quad (15)$$

where  $W = \text{diag}(w^{(1)} w^{(2)} \dots w^{(L)})$  is the weight matrix and  $w^{(i)}$  is the weight for the  $i$ -th link. The weights of links are calculated based on the average mean square errors in the first round. Suppose the error of the  $i$ -link is  $\text{err}^{(i)}$ , the weights of links with first 4 smallest errors are set to 1 to ensure enough independent equations for least square method, and the weights of rest links are updated as:

$$w^{(i)} = e^{-\zeta(\text{err}^{(i)} - \text{err}_{\min})} \quad (16)$$

where  $\zeta$  controls the extent of suppressing, and  $\text{err}_{\min}$  is the smallest link error.

## 6 EVALUATION

### 6.1 Experiment Methodology

**Implementation.** We implement *Widar* using three off-the-shelf mini-desktops (physical size 17cm x 17cm) equipped with Intel 5300 NIC. One mini-desktop with one external antenna works as the transmitter, while the other two mini-desktops, each with three external antennas, work as receivers. This provides 6 links in total for tracking. To obtain CSI measurements from Wi-Fi data frames, all mini-desktops are installed with the Linux 802.11n CSI Tool [4] and set up to inject in monitor mode on Channel 161 at 5.825 GHz. A high transmission rate of 2000 Hz is adopted, for comparing the effects of different sampling rates via downsampling.

**Evaluation Setup.** Figure 6 shows the deployment schemes of *Widar*. Specifically, two types of schemes are designed, where

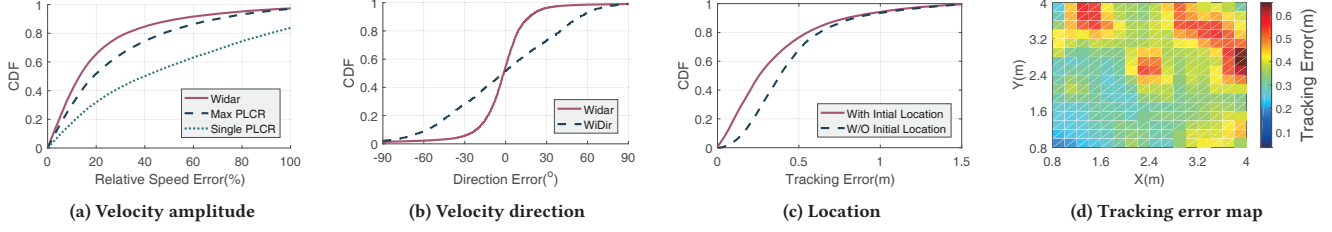


Figure 8: Overall performance of velocity and location tracking

devices are deployed at the corner (**Setup 1**), and where devices are deployed at one side (**Setup 2**). The tracking area is a 4 m × 4 m square. We design traces with various lengths, directions and shapes (such as line, curve, rectangular, circle and fold line, etc.), and test them with 5 volunteers. **The volunteers include 4 males and 1 female**, with heights in the range of **1.6 m to 1.8 m**, and ages in the range of **20 to 35**. **Code and data samples are available at our official website**<sup>1</sup>.

**Ground Truth.** To obtain the ground truth locations and velocities of human trajectories, we install a Canon 70d digital camera to record walking videos and extract traces using video-based tracking. The camera frames the experimental area from a field of view as shown in Figure 7 and generates FHD (1920×1080) videos at a rate of 25 fps. The visual tracking algorithm consists of two components. **First**, it identifies the tracking target in the video frame. To identify the tracking target, testers are asked to wear a light green T-shirt which produces high chromatic contrast against the background (e.g. wall and floor), as in Figure 7. **Second**, it transforms the pixel coordinates of the target to the world coordinates in physical space. **The transformation is performed based on the projection matrix** calculated from visual markers deployed in the experimental field.

The velocity output of *Widar* and ground truth are aligned by minimizing mean square error after alignment. The location outputs are aligned according to the corresponding velocity. Both velocity and location errors are calculated in a point-to-point manner.

روش نقطه به نقطه

## 6.2 Overall Performance

**Performance in Velocity Tracking** We first report performance of *Widar* on tracking target velocity, in terms of both speed and direction. For speed, we compare *Widar* with a naïve method: *Max PLCR*, which takes half the largest PLCR among all links as its estimate of target speed. In addition, we show the estimation errors when only one link is available (denoted *Single PLCR*). Figure 8a plots the CDF of relative speed errors of three methods over all trajectories. As illustrated, *Widar* achieves the highest accuracy with a median error of 13%, while those of *Max PLCR* and *Single PLCR* are 19% and 40% respectively. The favorable performance of *Max PLCR* attributes to the deployment of links, where links are deployed in two orthogonal directions in the experiment.

While both *Widar* and *Max PLCR* report highly accurate velocity amplitude, *Widar* further provides velocity direction, which is necessary for tracking. **We compare *Widar* with *WiDir*, which**

essentially calculates PLCR ratio of orthogonal links as target's moving direction. As shown in Figure 8b, *Widar* achieves an error within 18° for more than 80% measurements, while *WiDir* achieves only an error of 55°. The superior performance of *Widar* is due to its further consideration of location, rather than merely PLCRs as in *WiDir*.

**Performance in Location Tracking** Figure 8c shows the tracking error across all trajectories. As illustrated, with knowledge of accurate initial location, ***Widar* achieves high tracking accuracy with a median tracking error of 25 cm**. Without initial location, the performance slightly degrades yet **the median tracking error is still as low as 38 cm**. In addition, even without precise initial knowledge, **the 90-percentile tracking error is limited by 78 cm, guaranteeing decimeter-level accuracy**. Figure 8d shows the tracking error with respect to the reflection distances to the receivers with a map of the tracking area under the setup 1. As shown, when the target is close to the link (i.e. the origin and two axes), *Widar* achieves higher accuracy with average error of 20 cm. Accuracy degrades when the target moves away from the link. The tracking error is maximized on the side opposite to the links. These trends are caused by two factors: the drop of SNR of the reflecting signal, and the decrease of PLCR of the reflecting paths. As a result, the coverage of single *Widar* system is limited. However, it can still be extended by deploying multiple cooperative *Widar* systems.

Currently, *Widar* requires intensive computations for initial location estimation and opportunistic calibration, which may limit the scalability of *Widar*. Thus, location hints obtained by certain passive localization techniques, even not accurate enough, may benefit *Widar* for tracking. **Fortunately, the advent of passive localization works [8, 16] make it possible. For example, Dynamic-MUSIC [8] estimates angle of arrival (AoA) of moving targets**, which may complement *Widar* by reducing searching range of initial location and opportunistic calibration. We plan to integrate both AoA and Doppler frequency shifts to achieve efficient and accurate passive tracking in future work.

## 6.3 Parameter Study

**Impact of walking direction.** We further explore how walking direction relative to the link impacts the accuracy of velocity estimation. Both transmitters and receivers are placed at one side of the tracking area, and testers are asked to walk in straight lines with various directions. As shown in Figure 9a, the performance of *Max PLCR* significantly decreases when the walking direction

<sup>1</sup> <http://tns.thss.tsinghua.edu.cn/wifiradar/WidarProject.zip>

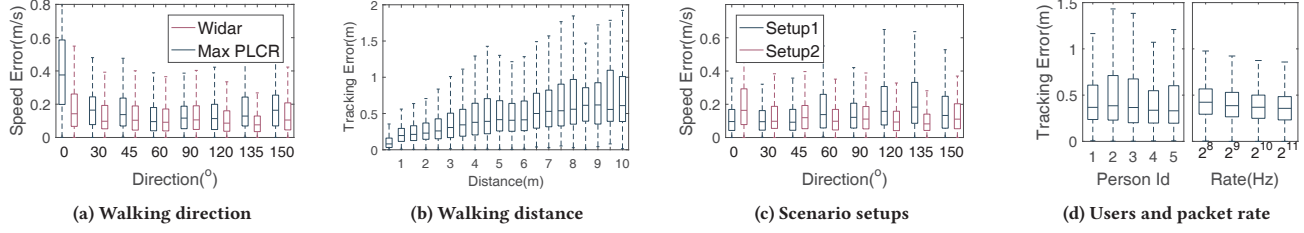


Figure 9: Impacts of different factors

is parallel to the link. In contrast, *Widar* achieves high accuracy through all walking directions. In conclusion, *Widar* successfully tracks velocity, while simply converting PLCR by a fixed rate as target speed leads to severe underestimation and high errors.

**Impact of walking distance.** Currently, *Widar* does not employ passive localization for calibration, it is interesting to examine the accumulative errors over different walking distances. As shown in Figure 9b, the tracking error accumulates at a moderate rate as the target continuously moves. Specifically, the median tracking errors increase from 10 cm to 61 cm when human continuously walks for 1 m to 10 m. While pseudo-calibration limits the accumulation rate of tracking error, it still requires occasionally pinpointing the target to avoid accumulation error. As current precise passive localization methods [8, 16] do not directly apply to *Widar*, we leave the development of the localization method for future work.

**Impact of deployment.** As different deployment of links may impact the tracking accuracy, we design two deployment schemes as in Figure 6 and evaluate the performance under individual setting. Specifically, in Setup 1, the transmitter is placed at the corner of the tracking area, and two receivers are deployed along two sides adjacent to that corner. In Setup 2, all devices are placed at one side of the tracking area, where the transmitter is placed in the middle and two receives are placed at opposite sides of the transmitter. Testers are asked to walk in straight lines with various directions. As shown in Figure 9c, while *Widar* achieves consistent accuracy across all directions under both deployments, the error distributions with the two deployments are apparently different. Specifically, the direction with maximum error in Setup 1 is 135°, and that in Setup 2 is 0°, which is the direction almost in parallel with all links.

**Impact of human diversity.** To determine whether *Widar* consistently works for different users, we recruit five volunteers to participate in experiments. The five volunteers have different ages (from 20~30), heights (1.6 m~1.8 m) and genders. Except for one participant who helped develop the prototype, the other four volunteers were for the first time taking part in the experiment without training. Figure 9d plots the tracking errors of *Widar* with different tracking targets. As shown, *Widar* tracks all targets with high precision, without knowing any body features of the targets.

**Impact of packet transmission rate.** Initially, we set the packet transmission rate to 2000 Hz and interpolate CSI measurements to 2048 Hz. To evaluate the impact of different transmission rates, we test *Widar* with down-sampled CSI measurements of 1024, 512, 256 Hz. Theoretically, decreasing sampling rate may

aggravate aliasing effect of the spectrogram as the high-frequency power aliases with target-frequency power, which leads to increase in PLCR estimation error. However, as shown in Figure 9d, the tracking accuracy of *Widar* only slightly decreases, as the sampling rate exponentially decreases from 2048 Hz to 256 Hz. The counter-intuitive results indicate that the major power of CSI measurements concentrates at the low end of spectrum, and a transmission rate of 250 Hz is sufficient for tracking human walking.

## 7 RELATED WORK

**RF-based Active Tracking.** Active motion tracking, which essentially localizes radio devices attached on objects, has been studied in depth. Various signal features, from RSSI [27] to CSI [13], have been exploited as location fingerprints. Incorporating inertial sensors embedded in mobile devices exposes a new way for localization tracking [12]. However, inertial sensors can only be used as step counter due to unknown drifts and changing device orientation [5].

Other active motion tracking systems are built upon phased antenna arrays [24]. SpotFi [7] jointly estimates AoA and ToF of the incident signal by synthesising sensors at sub-carrier level. However, these tracking schemes require dedicated radio devices that expose accurate phase information of antenna array, which is unavailable in COTS Wi-Fi devices due to unknown phase calibration factors [18].

**RF-based Passive Motion Tracking.** Passive motion tracking exploits reflections of signals to recognize and localize moving objects. Isolating certain reflections can be done in either time domain [9] or frequency domain [1, 2]. WiVi [3] proposes a MIMO interference nulling algorithm to focus the receiver on moving targets. In contrast, however, isolating certain reflections can not be processed on COTS Wi-Fi devices due to limited bandwidth, constant carrier frequency and asynchronous between transmitter and receiver.

*Widar* is similar to conventional Doppler radar, yet it develops finer tracking model to consider location differences of transceivers and accurately relate target's radial velocity with Doppler frequency shifts. Further, *Widar* works on COTS WiFi devices, where it recovers the signs of Doppler frequency shifts using subcarrier correlations and human motion continuity. Finally, *Widar* targets multipath-rich indoor environments, and adopts novel algorithms to filter and extract target Doppler frequency shift from noisy CSI measurements.

Recently, mTrack [21] designs a mmWave radio system to track writing objects with signal phase shifting. WiDeo [6] jointly estimates ToF and AoA to identify all reflectors and extract moving ones by comparing successive estimation. Tadar [26] tracks human motion by extracting phase of signals reflected off human body. WiDraw [14] tracks in-air hand motion by computing AoA of blocked incident signals. D-Watch [17] tracks human by identifying AoA of RFID tags' backscatter signal blocked by human. Similarly, phase information used in these tracking systems is unavailable in COTS Wi-Fi devices.

Recent techniques achieve decimeter-level passive localization using COTS Wi-Fi [8, 16]. LiFS [16] leverages shadowing effect of targets near LoS of links and requires dense deployment of devices. Dynamic-Music [8] leverages the incoherence between reflecting signal and static signal to separate reflecting signal and estimate its AoA. Thus it requires pre-calibration of NICs and strictly shaped antenna array. In contrast, *Widar* targets at more practical scenarios where only a few devices are casually deployed on area edges.

**Wi-Fi-based Gesture and Activity Recognition.** Wi-Fi-based activity recognition attracts considerable research interests recently. Many innovative applications and systems have been designed, including gesture recognition [19], respiration detection [22] and direction estimation [11], etc. These works mainly target at activity recognition instead of location tracking and speed estimation. As such, most of them employ learning-based solutions for recognition. WiSee [10] leverages Doppler effect to enable gesture recognition using specialized hardwares (USRP). CARM [18] uses off-the-shelf Wi-Fi NICs and correlates CSI value dynamics with human motion, yet without velocity. In this paper, *Widar* further reveals the relationships of CSI dynamics and real human moving velocity. In addition, *Widar* targets movement tracking and enables simultaneous estimation of human velocities and locations.

## 8 CONCLUSION

In this paper, we propose a Wi-Fi-based passive tracking system *Widar* that simultaneously estimates human's location and velocity at decimeter level. First we build a model that geometrically quantifies the relationships between CSI dynamics and human mobility. Then we propose several novel techniques to translate this model into a fine-grained tracking system. We implement *Widar* on COTS Wi-Fi devices and evaluate it in real environments. Experimental results show that *Widar* achieves decimeter-level accuracy with a median location error of 25 cm and 38 cm with and without initial positions and a median relative velocity error of 13%. Future work focuses on incorporating non-learning based localization and applying *Widar* to fortify various sensing applications.

## ACKNOWLEDGEMENT

This work is supported in part by the NSFC under grant 61522110, 61332004, 61472098, 61572366, 61602381, 61672319, 61632008, National Key Research Plan under grant No. 2016YFC0700100.

## REFERENCES

- [1] Fadel Adib, Zachary Kabelac, and Dina Katabi. 2015. Multi-person localization via rf body reflections. In *Proc. of USENIX NSDI*.
- [2] Fadel Adib, Zach Kabelac, Dina Katabi, and Robert C Miller. 2014. 3d tracking via body radio reflections. In *Proc. of USENIX NSDI*.
- [3] Fadel Adib and Dina Katabi. 2013. See through walls with wifi!. In *Proc. of ACM SIGCOMM*.
- [4] Daniel Halperin, Wenjun Hu, Anmol Sheth, and David Wetherall. 2011. Predictable 802.11 packet delivery from wireless channel measurements. *Proc. of ACM SIGCOMM* (2011).
- [5] Yonghang Jiang, Zhenjiang Li, and Jianping Wang. 2017. PTrack: Enhancing the Applicability of Pedestrian Tracking with Wearables. In *Proc. of IEEE ICDCS*.
- [6] Kiran Joshi, Dinesh Bharadia, Manikanta Kotaru, and Sachin Katti. 2015. Wideo: Fine-grained device-free motion tracing using rf backscatter. In *Proc. of USENIX NSDI*.
- [7] Manikanta Kotaru, Kiran Joshi, Dinesh Bharadia, and Sachin Katti. 2015. Spotfi: Decimeter level localization using wifi. In *Proc. of ACM SIGCOMM*.
- [8] Xiang Li, Shengjie Li, Daqing Zhang, Jie Xiong, Yasha Wang, and Hong Mei. 2016. Dynamic-music: accurate device-free indoor localization. In *Proc. of ACM UbiComp*.
- [9] Gerald Ossberger, Thomas Buchegger, Erwin Schimbäck, Andreas Stelzer, and Robert Weigel. 2004. Non-invasive respiratory movement detection and monitoring of hidden humans using ultra wideband pulse radar. In *Conference on Ultrawideband Systems and Technologies*.
- [10] Qifan Pu, Sidhant Gupta, Shyamnath Gollakota, and Shwetak Patel. 2013. Whole-home gesture recognition using wireless signals. In *Proc. of ACM MobiCom*.
- [11] Kun Qian, Chenshu Wu, Zimu Zhou, Yue Zheng, Zheng Yang, and Yunhao Liu. 2017. Inferring Motion Direction using Commodity Wi-Fi for Interactive Exergames. In *Proc. of ACM CHI*.
- [12] Souvik Sen, Jeongkeun Lee, Kyu-Han Kim, and Paul Congdon. 2013. Avoiding multipath to revive inbuilding WiFi localization. In *Proc. of ACM MobiSys*.
- [13] Souvik Sen, Božidar Radunovic, Romit Roy Choudhury, and Tom Minka. 2012. You are facing the Mona Lisa: spot localization using PHY layer information. In *Proc. of ACM MobiSys*.
- [14] Li Sun, Souvik Sen, Dimitrios Koutsonikolas, and Kyu-Han Kim. 2015. Widraw: Enabling hands-free drawing in the air on commodity wifi devices. In *Proc. of ACM MobiCom*.
- [15] Bo Tan, Karl Woodbridge, and Kevin Chetty. 2014. A real-time high resolution passive WiFi Doppler-radar and its applications. In *International Radar Conference*.
- [16] Ju Wang, Hongbo Jiang, Jie Xiong, Kyle Jamieson, Xiaojiang Chen, Dingyi Fang, and Binbin Xie. 2016. LiFS: Low Human Effort, Device-Free Localization with Fine-Grained Subcarrier Information. In *Proc. of ACM MobiCom*.
- [17] Ju Wang, Jie Xiong, Hongbo Jiang, Xiaojiang Chen, and Dingyi Fang. 2016. D-watch: Embracing "bad" multipaths for device-free localization with COTS RFID devices. In *Proc. of ACM CoNEXT*.
- [18] Wei Wang, Alex X Liu, Muhammad Shahzad, Kang Ling, and Sanglu Lu. 2015. Understanding and modeling of wifi signal based human activity recognition. In *Proc. of ACM MobiCom*.
- [19] Yan Wang, Jian Liu, Yingying Chen, Marco Gruteser, Jie Yang, and Hongbo Liu. 2014. E-eyes: device-free location-oriented activity identification using fine-grained wifi signatures. In *Proc. of ACM MobiCom*.
- [20] Bo Wei, Ambuj Varshney, Neal Patwari, Wen Hu, Thiem Voigt, and Chun Tung Chou. 2015. drti: Directional radio tomographic imaging. In *Proc. of ACM/IEEE IPSN*.
- [21] Teng Wei and Xinyu Zhang. 2015. mtrack: High-precision passive tracking using millimeter wave radios. In *Proc. of ACM MobiCom*.
- [22] Chenshu Wu, Zheng Yang, Zimu Zhou, Xuefeng Liu, Yunhao Liu, and Jiannong Cao. 2015. Non-Invasive Detection of Moving and Stationary Human With WiFi. *Selected Areas in Communications, IEEE Journal on* (2015).
- [23] Dan Wu, Daqing Zhang, Chenren Xu, Yasha Wang, and Hao Wang. 2016. WiDir: walking direction estimation using wireless signals. In *Proc. of ACM UbiComp*.
- [24] Jie Xiong and Kyle Jamieson. 2013. ArrayTrack: a fine-grained indoor location system. In *Proc. of USENIX NSDI*.
- [25] Fan Yang, Qiang Zhai, Guoxing Chen, Adam C Champion, Junda Zhu, and Dong Xuan. 2016. Flash-Loc: Flashing Mobile Phones for Accurate Indoor Localization. In *Proc. of IEEE INFOCOM*.
- [26] Lei Yang, Qiongzhen Lin, Xiangyang Li, Tiansci Liu, and Yunhao Liu. 2015. See through walls with cots rfid system!. In *Proc. of ACM MobiCom*.
- [27] Zheng Yang, Chenshu Wu, and Yunhao Liu. 2012. Locating in fingerprint space: wireless indoor localization with little human intervention. In *Proc. of ACM MobiCom*.
- [28] Zheng Yang, Zimu Zhou, and Yunhao Liu. 2013. From RSSI to CSI: Indoor localization via channel response. *ACM Computing Surveys (CSUR)* (2013).
- [29] Jungwon Yoon, Hyung-Soo Park, and Diane Louise Damiano. 2012. A novel walking speed estimation scheme and its application to treadmill control for gait rehabilitation. *Journal of neuroengineering and rehabilitation* (2012).